

# Feasible use of municipal solid waste incineration bottom ash in ultra-high performance concrete

Peiliang Shen, Haibing Zheng, Dongxing Xuan, Jian-Xin Lu\*, Chi Sun Poon\*

The Hong Kong Polytechnic University, Department of Civil and Environmental Engineering,  
Hung Hom, Kowloon, Hong Kong

\*Corresponding author: cecspoon@polyu.edu.hk (C.S. Poon); jxinlu@polyu.edu.hk (J.X.  
Lu)

**Abstract:** In this study, municipal solid waste incineration bottom ash (IBA) was reused as fine aggregates to prepare ultra-high performance concrete (UHPC). The effects of IBA on the mechanical properties, workability, hydration, volume stability and microstructure of UHPC were investigated. The experimental results showed that the incorporation of an appropriate amount of IBA could improve the compressive strength of UHPC due to the internal curing effect. While the addition of excessive amount of IBA would reduce the strength significantly. From the microstructure analysis, the hydration of UHPC was promoted by adding IBA, leading to a higher hydration degree and denser microstructure of the paste compared to reference sample. The use of IBA in UHPC could effectively restrict the expansion due to the presence of metallic Al, glass, gypsum in the IBA as the UHPC matrix acted as a barrier in the vicinity of the IBA particles, which prevented the formation and propagation of cracks. Also, the highly impermeable UHPC cement paste, the use of supplementary cementitious materials and the high self-desiccation of UHPC further prevent the expansive chemical reactions from occurring. Thus, it was practicable to apply IBA in UHPC without considering the expansive risks and with easy pre-treatment, and it was demonstrated that the utilization of IBA in UHPC is a feasible solution for recycling IBA.

**Keywords:** UHPC; Incineration bottom ash; Expansion; Hydration; Microstructure

## 1. Introduction

Waste incineration is one of the most effective technologies for municipal solid waste (MSW) management [1]. Incineration bottom ash (IBA) is a kind of heterogeneous solid granular by products that is produced by using the incineration technology [2]. It has been reported that in China more than 400 modern MSW incinerations have been built until 2019 and more plants are on the way [3]. Hong Kong has also decided to build a 3000 tonnes/day incinerator which will be completed in 2024 [4]. Thus, a large amount of solid residues (mainly IBA) after incineration will be produced and pose environmental concerns [5]. In Hong Kong most solid wastes are mainly disposed at landfills [4]. Since landfill sites are running out and natural resources such as sand and crushed rocks are becoming scarce in the vicinities of major cities, the possible reuse of IBA as construction and building materials is recently attracting more attentions.

Generally, IBA consists of glass, minerals, ceramics, magnetic and paramagnetic metals, slag phase and unburned materials etc. [6]. Most of the previous research studies focused on reusing IBA as replacements of aggregates in road-subbase or low grade concrete blocks [1, 7, 8]. However, the application of IBA in concrete was quite limited as pretreatments are needed to improve its properties [9]. The challenges to utilize the IBA in the construction field include: heavy metals and salts leaching of IBA [10], gas release due to the presence of metallic aluminum [11], potential alkali-silica reaction (ASR) due to the presence of glass [12-14] and excessive formation of ettringite due to the rich sulphate content [13-15]. Because these challenges would influence the performance of concrete or pose an environmental risk, these adverse effects need to be reduced before application of IBA in the concrete [16]. After applying in concrete, the heavy metals and salts leaching of crushed concrete incorporating IBA was relatively low [11]. However, cracks induced by expansions due to the reaction of metallic Al, ASR of glass and excessive formation of ettringite could adversely deteriorate the performance of concrete [12-15].

In order to promote the reuse of IBA in concrete, many pre-treatment techniques have been explored. Treatment methods such as washing, carbonation, air and thermal treatments as well as separation and removal of ferrous and non-ferrous metals were proved to improve the engineering properties and reduce chemical attack [17-20]. Among the above, alkaline pre-treatment methods were considered to be the effective in removing the metallic materials [21-23]. However, these treatment processes are usually either time consuming or costly, which are difficult to be applied in practice.

Recent studies show the use of dry mixing method, reduced water to cement ratio and additions of supplementary cementitious materials (SCMs) (fly ash, ground granulated blast-furnace slag, silica fume and glass powder) have potentials to reduce the deleterious expansion of the concrete prepared with the incorporation of IBA [13, 24]. However, these approaches still cannot completely prevent the detrimental effects caused by IBA. Thus, a high-efficiency and environmental-friendly method is essential to be developed.

UHPC represents the development of advanced cementitious based materials, which possesses ultra-high mechanical properties and durability. It has the characteristics of very dense matrix and using high amounts of superfine SCMs. But UHPC exhibits very high autogenous shrinkage due to the high binder content [25]. But when IBA is used in UHPC, this may be beneficial to compensate for the expansion caused by IBA. In addition, as the relative humidity in UHPC is low [26], the chemical reactions causing expansion may be hindered due to a lack of free moisture. However, the performance and potential cracking deterioration of UHPC incorporating with IBA is still unclear. This study aims at quantifying the effect of using IBA as replacement of quartz sand on the performance of UHPC.

## 2. Materials and method

### 2.1 Materials

ASTM type I ordinary Portland cement (OPC) from Green Island Cement (Holdings) Limited, silica fume (SF) from Elkem and fly ash (FA) from a Hong Kong coal fired power station were used. The oxide compositions and physical properties of these cementitious materials were presented in Table 1. A commercially sourced quartz sand with a size of 0.15-1.18 mm was used as aggregates for UHPC. The IBA was collected from a MSW incineration plant and sieved to the size of 0.15-1.18 mm was used to systemically (0%, 25%, 50%, 75% and 100%) replace the quartz sand. The content of metallic Al in IBA was 0.19% which was tested according to the previous study [13]. The portlandite consumption of IBA was 189.2 mg of  $\text{Ca}(\text{OH})_2$  per gram of the IBA obtained by using the modified Chapelle test [27]. The oxide compositions of IBA was showed in Table 1. Also the main crystalline phases of IBA were quartz, calcite and calcium-sodium-magnesium phosphate, which was obtained from the X-ray diffraction analysis method. The physical properties of binders and aggregates were shown in Table 2. A polycarboxylate ether (PCE) high range water reducer from BASF and tap water were used for mixing. A straight steel fiber with a diameter of 0.22 mm and a length of 13 mm was used as received.

Table 1 Oxide compositions of binders and IBA (wt. %)

Oxide	$\text{SiO}_2$	$\text{Al}_2\text{O}_3$	$\text{CaO}$	$\text{Fe}_2\text{O}_3$	$\text{SO}_3$	$\text{MgO}$	$\text{Na}_2\text{O}$	$\text{K}_2\text{O}$	LOI
Cement	19.37	3.92	66.30	3.69	2.81	1.61	0.13	0.59	1.09
Silica fume	88.29	0.14	0.92	0.19	1.51	3.21	0.14	0.17	5.26
Fly ash	54.69	12.71	17.48	4.61	0.97	1.68	1.75	3.18	1.79
IBA	49.60	11.00	17.3	5.36	1.15	2.09	6.04	1.63	—

Table 2 Physical properties of binders and aggregates

Properties	Blaine fineness (m <sup>2</sup> /kg)	Density (g/cm <sup>3</sup> )	Water Absorption (%)	Setting time (min)	
				Initial	Final
Cement	345.0	3.15	/	237	298
Silica fume	15248.0	2.61	/	/	/
Fly ash	456.5	2.20	/	/	/
Quartz sand	13.2	2.59	0.54	/	/
IBA	2274.6 (BET)	2.10	7.4	/	/

## 2.2 Preparation of UHPC incorporating IBA

During mix proportion formulation, the principle of compressive packing model was used to improve the performance of UHPC. Specifically, the modified Andreasen and Andersen model was used to design the mix proportions of UHPC by obtaining optimal packing of the particles including cement, fly ash, quartz sand and IBA [28]. The modified Andreasen and Andersen model acted as a target function for optimizing the mixture proportion of UHPC. An optimal mix proportion of each binder could be achieved by fitting the designed mix and target curves with a partition coefficient of 0.23 [29]. When the deviation between the target curve and the mix was minimized by using the Least Squares Method, the solid mix compositions of UHPC could be obtained and considered as the best one [29]. The Particle size distributions of raw materials, target and optimized curves were shown in Figure 1. In this study, a IBA with the same size range was used to replace the corresponding quartz sand. The water to binder ratio and the dosage of PCE were adopted, aiming at obtaining a good workability. Thus, the mix proportions of UHPC with and without are shown in Table 2.

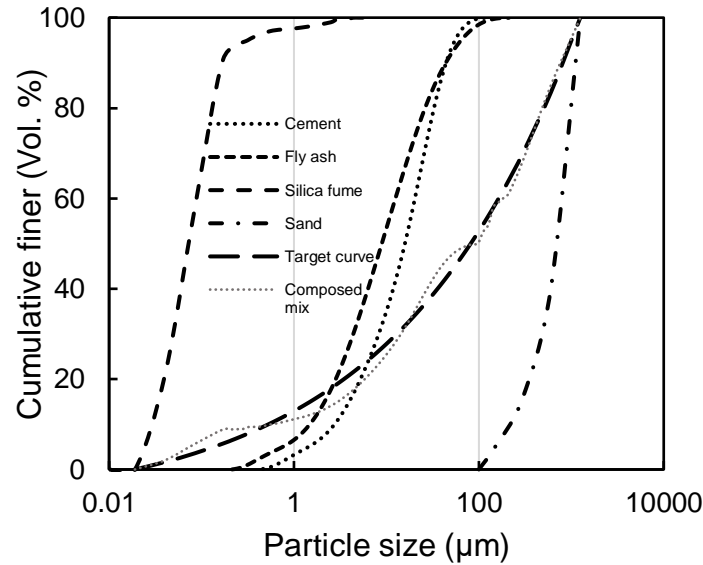


Figure 1 Particle size distributions of the ingredients, target and optimized curves of UHPC mixtures

Table 2 Mix proportions of UHPC mixtures (kg/m<sup>3</sup>)

No.	Cement	Fly ash	Silica fume	Quartz sand	IBA	Water in IBA	w/b	PCE dosage
F0	640	160	176	1000	0	0	0.18	32
F25	640	160	176	750	202.5	15.0	0.18	32
F50	640	160	176	500	405	30.0	0.18	32
F75	640	160	176	250	607.5	45.0	0.18	32
F100	640	160	176	0	910	60.0	0.18	32

The high water absorption characteristic of IBA was firstly addressed by immersing the IBA in water for 24 h, then it was made to the surface dry condition before use. The binders including OPC, fly ash and silica fume were firstly dry mixed using a laboratory pan mixer for 3 minutes at low speed. Afterwards, the water and superplasticizer were added into the mixer, then it mixed for 2 minutes at low speed and another 3 minutes at high speed. Finally, the aggregates including quartz sand, IBA in the surface dry condition prepared above, and 2% steel fibers by volume were added and mixed for 2 minutes at high speed and 1 minute at low speed. After that,

the fresh mixture was cast into the steel molds and vibrated on a vibration table for 1 minute. The UHPC specimens were demolded after 24 hours and cured under a sealing condition at  $20\pm1$  °C.

## 2.3 Test methods

### *2.3.1 Compressive strength*

The UHPC specimens with the size of 40 mm×40 mm×160 mm were prepared to determine the compressive strength of UHPC. All the samples were demolded at 24 h and cured at  $20\pm1$  °C under the sealing condition. A compression machine with a maximum load of 300 kN was applied. A loading rate of 0.6 MPa/s was used for the compressive strength measurement. Three samples for each mixture were measured to obtain the average value.

### *2.3.2 Density and workability*

The density of UHPC incorporated different amounts of IBA was tested according to ASTM C 1754 [30]. Three specimens were tested to obtain the average value.

The slump flow of UHPC was measured according to BS EN1015 [31]. The spread diameters of the fresh UHPC mixtures were determined after mixing.

### *2.3.3 Isothermal conduction calorimetry*

An I-Cal 4000 isothermal calorimeter was used to test the normalized heat flow and cumulative heat of UHPC incorporated different amounts of IBA. For each mixture, about 50 g of UHPC mixture was weighted into a plastic container and placed into the calorimeter to monitor the heat flow and cumulative heat. The measurement was started at 15 minutes after mixing and recorded for 168 hours at  $20\pm0.1$  °C.

### *2.3.4 Dry shrinkage and expansion in NaOH solution*

The dry shrinkage of UHPC incorporating with different amounts of IBA was determined according to modified British Standard (BS ISO-Part 8, 2009) [32]. The samples with the size of 25 mm×25 mm×285 mm were prepared for the shrinkage measurement. The specimens were

demolded at 24 hours and cured for another 48 hours at room temperature, then they were stored in an environmental chamber with a temperature of 23 °C and a relative humidity of 50 %. A contact deformation tester was used to test the dimensional length the specified days. The dry shrinkage was recorded until 42 d.

The expansion behavior of UHPC incorporating with IBA was measured according to ASTM C 1260 [33]. The UHPC bars with the size 25 mm×25 mm×285 mm were used. After demolding at 24 hours, the specimens were placed into a hot water (80 °C) bath and cured for 24 hours. The initial length was recorded before immersing in the hot NaOH solution. Afterwards, they were immersed in 1 mol/L hot NaOH solution (80 °C). The expansion values were recorded at 1 d, 3 d, 7 d, 14 d, 21 d and 28 d, respectively.

### *2.3.5 Pore structure*

The pore structure of UHPC incorporated different amounts of IBA was measured by using mercury intrusion porosimetry (MIP) by an AutoPore IV 9500 series pore size analyzer (Micromeritics Instrument Corporation). The thin pieces cut from the UHPC samples were used for the measurement. Before use, the hydration was stopped at 28d by placing into ethanol, and dried in a vacuum oven at 60 °C for 48 h. The contact angle between the pore surface and mercury was set at 130 °.

Nitrogen adsorption and desorption isotherms of UHPC incorporated different amounts of IBA and IBA were measured by an accelerated surface area and porosimetry system (Micromeritics ASAP 2020). A temperature of 60 °C was set for the measurement. The pore structure of UHPC with the size ranging between 2 nm and 200 nm could be obtained.



### 2.3.6 Thermogravimetric analysis

The hydration of UHPC were stopped at the age of 28 d by placing into ethanol. Then they were dried and grounded into powder with a particle size smaller than 75  $\mu\text{m}$ . Then, about 10 mg of the samples was used for the thermogravimetric (TG) analysis (Rigaku, Thermo plus EVO2). The thermogravimetric analysis was conducted from 40  $^{\circ}\text{C}$  to 1000  $^{\circ}\text{C}$  at a heating rate of 10  $^{\circ}\text{C}/\text{min}$  under a nitrogen atmosphere. Before the test, the specimens were dried in a vacuum oven.

### 2.3.7 Scanning electron microscopy (SEM)

The UHPC samples at the curing age of 28 d were selected for the microstructural analysis. Before the sample preparation, the hydration of all the specimens were stopped by immersing in ethanol for 24 hours and dried in a vacuum oven. A scanning electron microscope fitted with a BSE detector (model VEGA3, TESCAN) was used to capture SEM and backscattered electron imaging (BSE) images. The SEM and BSE tests were operated at an accelerating voltage of 20 kV and 15 kV, respectively. For the SEM imaging, fractured surface specimens were taken from the inner part of UHPC samples. For the BSE observations, thin slices were cut from the cubic samples and mounted into an epoxy resin. The specimens were firstly polished with 600, 800, 1200 and 2500 grit polishing papers, and then they were polished with diamond abrasives with the size of 3  $\mu\text{m}$ , 1  $\mu\text{m}$  and 0.25  $\mu\text{m}$ .

### 2.3.8 Micro-hardness

The hydration of UHPC were stopped at the age of 28 d by placing into ethanol, and the specimens with a thickness of 3 mm were chosen and mounted into an epoxy resin, followed by the polishing procedures described Section 2.2.7. A digital micro-hardness tester (HVX1000A, China) equipped with a Vickers diamond pyramid indenter was used. A load of 25 gf was selected

186 and a dwell time of 10 s was applied. For each specimen, 100 indentations were made to calculate  
187 the average value.

## 188 3. Results and discussion

### 189 3.1 Compressive strength

Figure 2 shows the effect of IBA incorporation on the compressive strength of UHPC as a function of curing time. It could be observed that incorporating 25% IBA in the UHPC led to a slight increase of compressive strength at the curing age of 28 d, but the compressive strength decreased obviously with the continuous increase of IBA. The compressive strength of UHPC was reduced by over 20.9% compared to that of the reference sample when the IBA replacement ratio was 100%. Even so, the strength was still higher than 130 MPa. It should be noted that the compressive strength of the reference sample attained the maximum strength value at the curing age of 3 d, whereas the 28 d-compressive strength of UHPC incorporating with a small amount of IBA (25%) was improved at the later age although the IBA had a high porosity. This is different from the results reported in a previous study [34]. The enhancement of compressive strength was probably due to the internal curing effect of IBA, which is similar to the internal curing effect of lightweight aggregate in UHPC [35, 36]. The internal curing of IBA also improved the internal humidity and promoted the hydration degree of UHPC, which contributed to the improvement of compressive strength [26]. However, the presence of porous IBA would increase the total porosity of UHPC, which would certainly adversely affect the compressive strength. When the IBA content was low (25%), the enhancement of compressive strength due to internal curing might be higher than the reduction of compressive strength due to adverse effect of the porous IBA. So the 28 d-compressive strength of UHPC incorporating 25% IBA possessed the highest value.

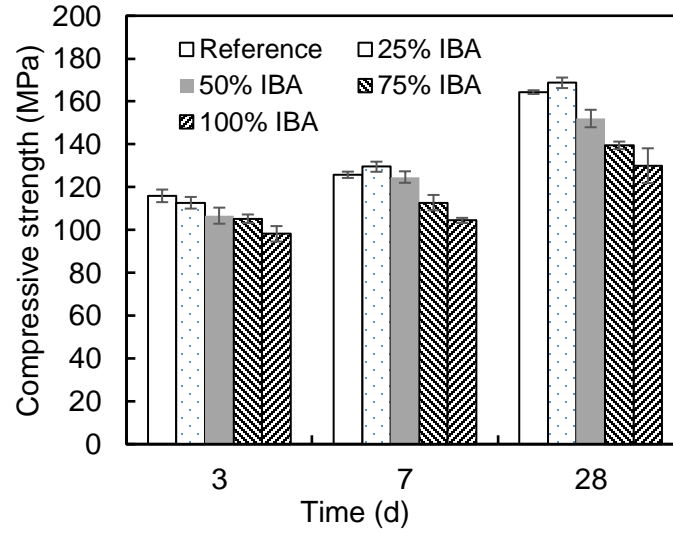


Figure 2 Effect of IBA on the compressive strength of UHPC

### 3.2 Workability and density

Figure 3 shows the influence of IBA replacement on the workability and density of UHPC. It can be noticed that the addition of IBA reduced the density of UHPC obviously. This was because the dry density of IBA ( $2100 \text{ kg/m}^3$ ), was lower than that of quartz sand ( $2590 \text{ kg/m}^3$ ). So the relationship between addition of IBA and density of UHPC is almost linear. In addition, although the total water to binder ratio of UHPC was significantly increased by using IBA, the slump flow values were almost similar. This indicates that the presoaked IBA did not have a negative influence on the workability of UHPC. As a result, the UHPC incorporating different amounts of IBA showed desired workability.

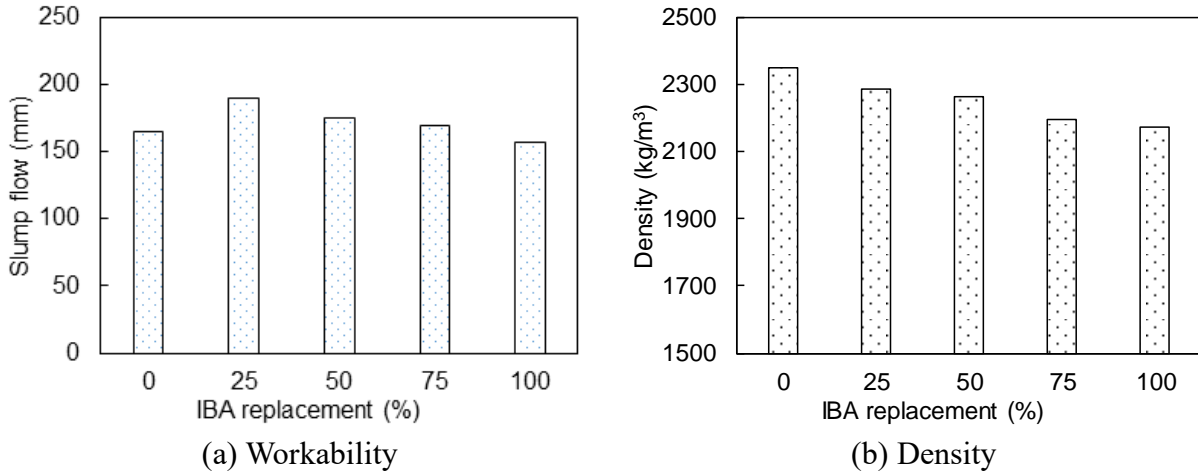


Figure 3 Effect of IBA on the slump flow (a) and density (b) of UHPC

### 3.3 Volume stability

The dry shrinkage of UHPC incorporating different amounts of IBA are shown in Figure 4. It can be observed that the dry shrinkage was obviously influenced by the addition of IBA, and it increased with the increasing amount of IBA. This is different from the effect of internal curing materials on the autogenous shrinkage of UHPC [37-39], where the total autogenous shrinkage would be reduced [38, 39]. However, in the present case, the presoaked water in IBA was also released before setting [26], which increased the water to binder ratio of the cement paste rather than for internal curing, leading to a higher drying shrinkage [40]. It can be concluded that the presence pre-wetted IBA contributed to the increased dry shrinkage of UHPC.

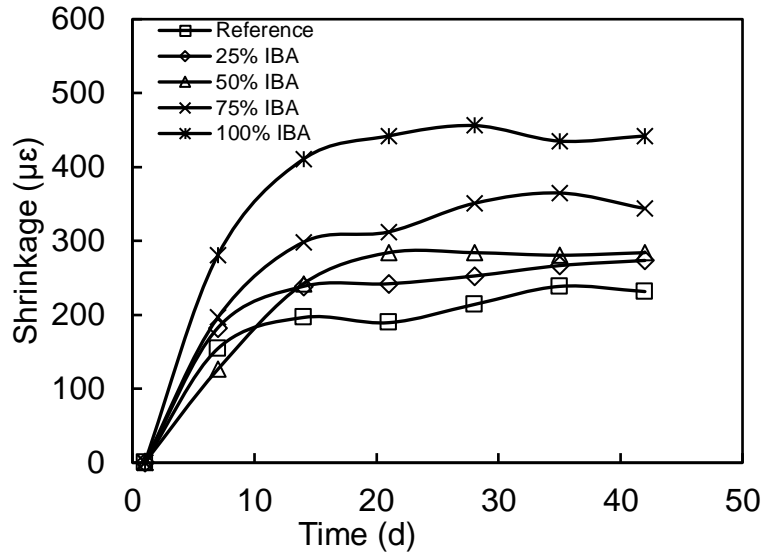


Figure 4 Dry shrinkage of UHPC incorporating with different amounts of IBA

The expansion behavior of UHPC incorporating with different amounts of IBA was tested according to ASTM C 1260 [33]. The results are shown in Figure 5. It can be seen that the length changes of UHPC shifted from shrinkage to expansion as the content of IBA increased. A maximum expansion value of 196.5  $\mu\epsilon$  was obtained at 28 d when 100% quartz sand was replaced by IBA. In the case of UHPC prepared without IBA, the hydration was promoted by immersing in the hot NaOH solution, so the UHPC shrank and the shrinkage increased with curing time. It should be noted that the UHPC still shrank when the replacement ratio of IBA was lower than 50%.

When IBA was present in the matrix, the components in IBA such as metallic Al and glass would react with NaOH to produce  $H_2$  gas or ASR gel leading to the expansion stress [41, 42]. In addition, the presence of gypsum in the IBA could also react with aluminate phases in the cement to cause expansive reactions. Therefore, expansive behavior was observed when the content of IBA was larger than 50% in the UHPC.

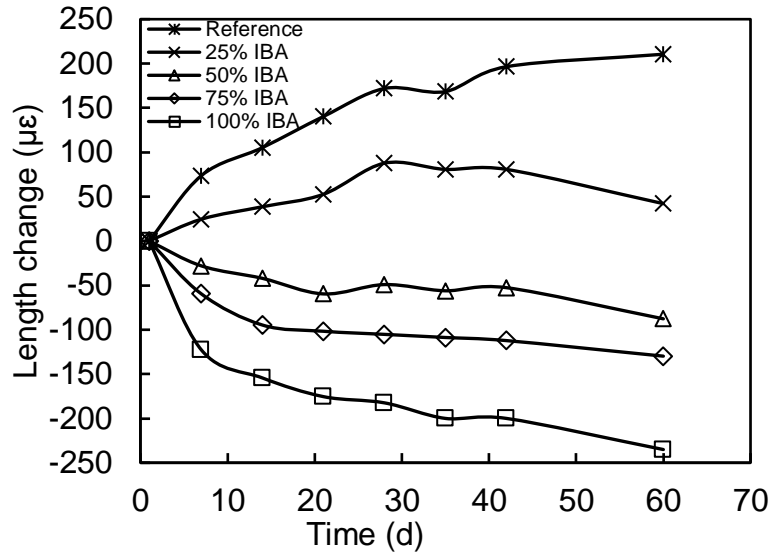


Figure 5 Length changes of UHPC in NaOH solution

### 3.4 Heat of hydration

The influence of IBA on the hydration of UHPC is presented in Figure 6. The heat flow and cumulative heat are normalized by the weight of cementitious materials. It can be observed that the addition of IBA obviously altered the heat evolution of UHPC at the early age. Firstly, the dormant period was shortened after adding IBA, and it trended to decrease with increasing content of IBA. Because the dormant period of UHPC was usually related to the water to cement ratio, content of superplasticizer and characteristic of cement etc. [37, 43, 44], the change of the dormant period seemed to be caused by the water desorption of IBA and ion dissolution of IBA [24]. Secondly, the main peak followed by the accelerating period shifted from 48 h to 15 h when the IBA replacement was increased from 0% to 100%. Thirdly, a higher amount of cumulative hydration heat was recorded for the UHPC incorporated with IBA. Thus, the IBA not only accelerated the hydration of UHPC but also increased its hydration degree. This is mainly attributed to the internal curing effect of IBA. Because the IBA was presoaked in water before use, some water in IBA would be released during hydration, which led to the enhancement of relative

humidity. According to a previous study [26], the initial relative humidity of fresh UHPC was lower than 100%, thus the water in the IBA could be released immediately after mixing. As a result, the water to binder ratio was increased and the hydration process was changed accordingly. As the hydration proceeded, the water desorption of IBA would continue to produce a higher relative humidity. This internal curing effect would promote the hydration of UHPC. Overall, the water release of IBA in UHPC played a main role in controlling the hydration process, resulting in a higher hydration degree [45, 46].

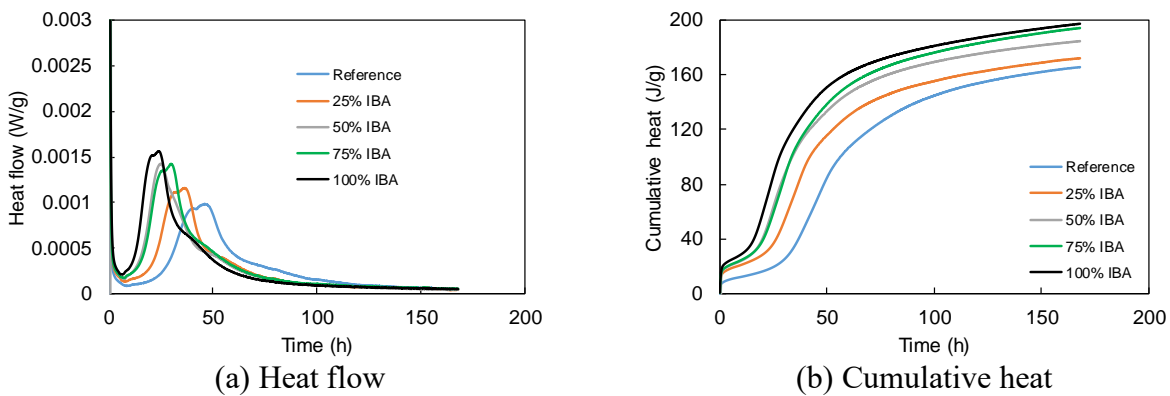


Figure 6 Heat flow rate and cumulative heat of UHPC incorporating with different amounts of IBA

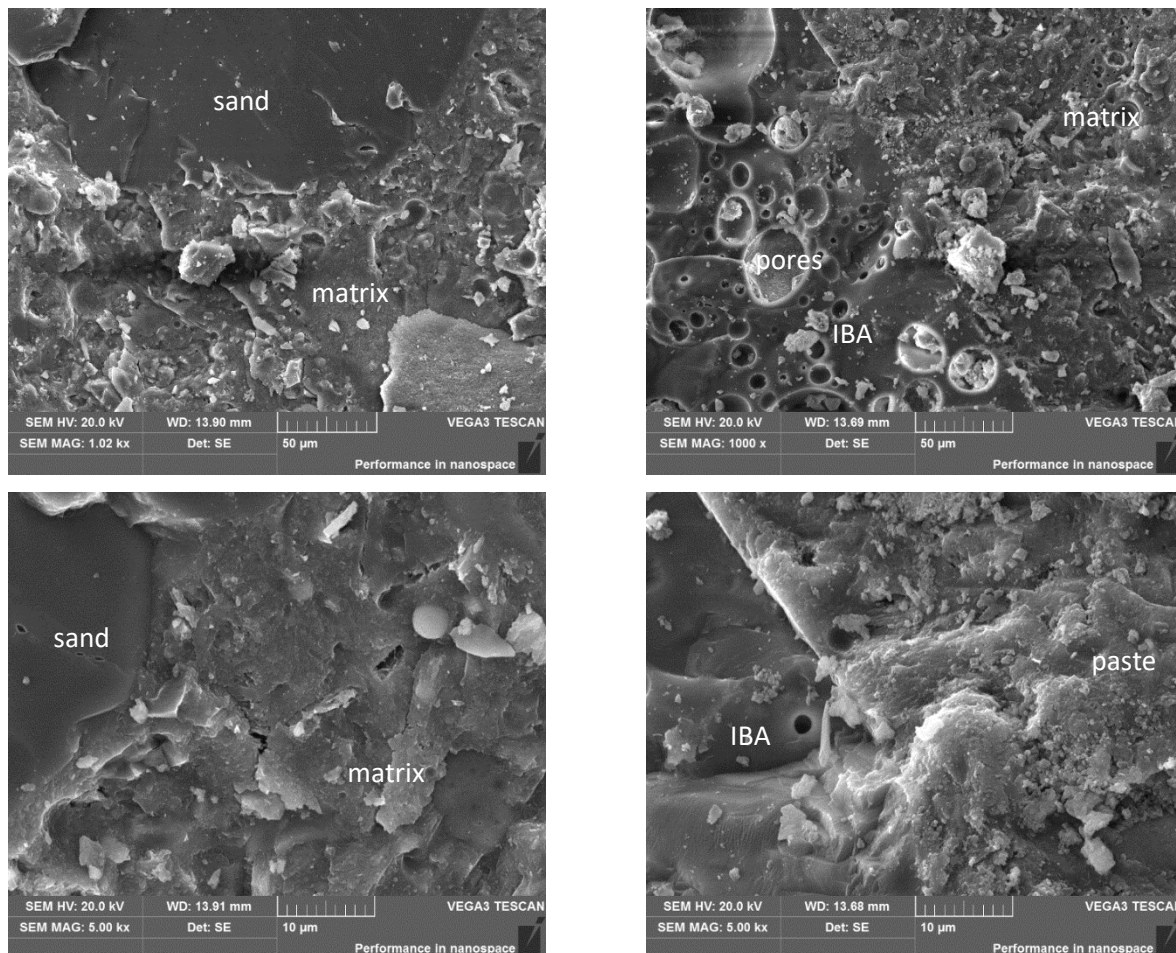
### 3.5 Microstructure

#### (1) SEM analysis

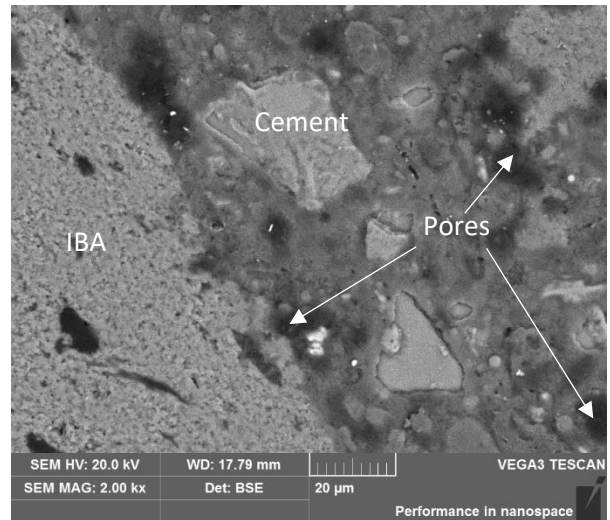
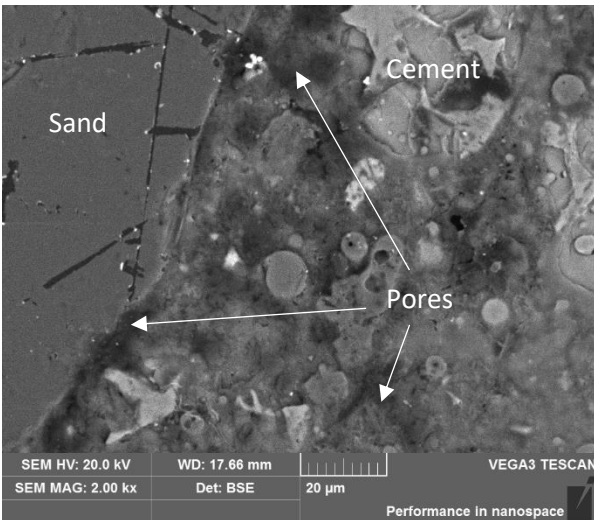
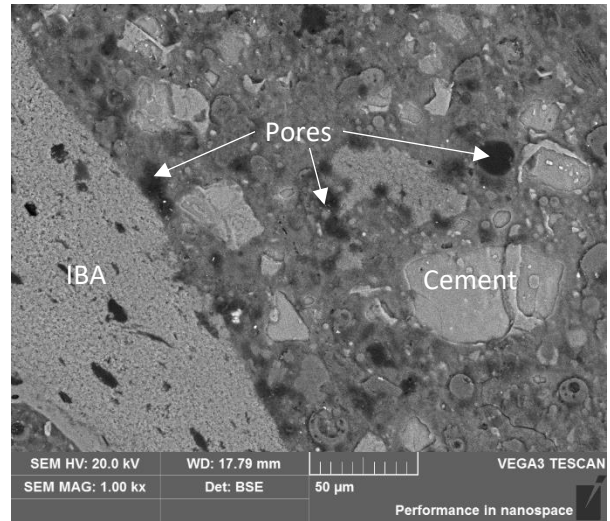
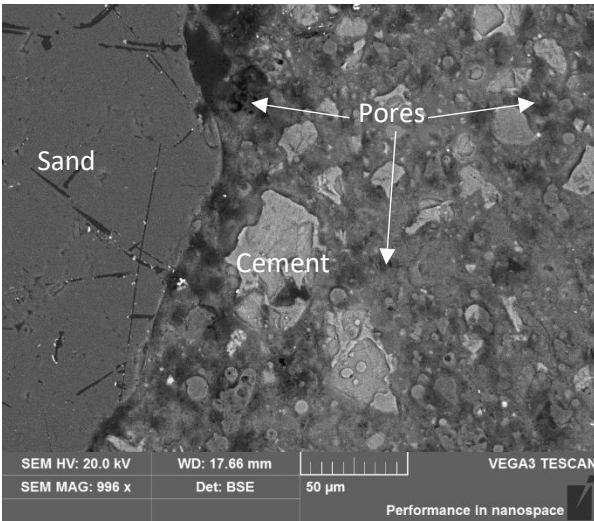
Figure 7 shows the microstructure of UHPC with and without IBA. For the control UHPC, a dense matrix could be observed. The interface between the aggregates (quartz sand and IBA) and the matrix was closely bonded, which indicated no obvious interfacial transition zone between the aggregates and the paste. It is believed that the presence of SCMs and a low water to binder ratio contributed to the dense interfacial transition zone [47]. Actually, the porous IBA was the weakest part in the UHPC, which would lead to a reduction in compressive strength. While for the UHPC incorporated low amount of IBA (less than 25%), the compressive strength was improved. So the application of IBA in UHPC shows two opposite effects on the mechanical properties



253 (porous structure vs internal curing). Also, these two effects would be enhanced by increasing  
 254 amount of IBA in UHPC. When the IBA content was less than 25%, the enhancement of  
 255 compressive strength due to internal curing overwhelmed the reduction of compressive strength  
 256 due to adverse effect of the porous IBA. However, for UHPC incorporating 50%, 75% and 100%  
 257 IBA, the reduction of compressive strength due to increased porosity is higher than the  
 258 enhancement of compressive strength due to internal curing. Thus, the compressive strength of  
 259 UHPC incorporating less than 25% IBA could achieve a higher value than that of the reference  
 260 sample.



(a) UHPC without IBA (b) UHPC incorporating 100% IBA  
 Figure 7 SEM images of the UHPC with and without IBA at 28 d



(a) UHPC without IBA

(b) UHPC incorporating 100% IBA

Figure 8 The BSE images of UHPC with and without IBA at 28 d

261

262

263

264

265

266

267

Figure 8 shows the BSE images on polished sections of UHPC with and without IBA. It can be observed that both samples showed dense microstructure. Also, there was a large amount of anhydrous cement clinker in both samples, indicating relatively low hydration degree. It can be seen that both sand and IBA were closely bound to the matrix. It should be noted that the cement paste around IBA was as dense as the matrix, and no visible interfacial transition zone could be found. Actually, the interfacial transition zone is usually the weakest zone in concrete and has a

great influence on the mechanical properties [48]. In this study, not only the presence of SCMs and a low water to binder ratio contributed to the dense interfacial transition zone [47] around aggregate. This good compatibility between matrix and IBA will be beneficial to the compressive strength of UHPC incorporated IBA.

## (2) Micro-hardness

According to a previous study [49], the matrix of UHPC incorporated internal curing materials had a lower porosity and higher compressive strength than that of normal UHPC due to the internal curing. Thus, the micro-hardness of the UHPC containing IBA was measured to characterize the change at the age of 28 d. In order to avoid the influence of different test areas on the measurements, 100 indentations were made to obtain the average value which represented the micro-hardness results of the whole matrix in UHPC. It can be observed from results in Figure 9 that the average micro-hardness of the matrix increased with the increase of IBA content. The average micro-hardness of the blank specimens was 112.78 HV and increased to 138.63 HV when the IBA replacement was increased to 100%. This enhancement of micro-hardness is mainly attributed to the internal curing effect, which results in higher micro-mechanical properties [48]. Therefore, although the addition of IBA incurred many weak zones in UHPC system, the incorporation of pre-soaked IBA could produce a harder matrix.

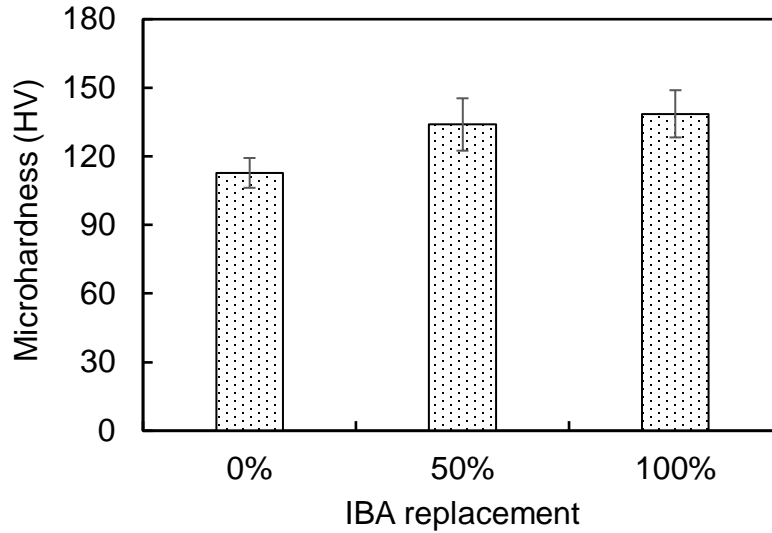


Figure 9 Micro-hardness of matrix in UHPC incorporating with different amounts of IBA

### (3) Thermal analysis

Figure 10 shows the TG and DTG curves of UHPC after curing for 28d . Four main mass losses could be observed in TG curves. The first mass loss around 100 °C was attributed to the water unbounded and bounded in the hydrates (such as C-S-H, AFt and AFm) [50, 51]. The mass loss around 450 °C was due to the dehydroxylation of  $\text{Ca}(\text{OH})_2$  [52, 53]. The mass loss around 650 °C referred to the decarbonation of  $\text{CaCO}_3$ . The mass loss around 850 °C referred to the transformation of  $\text{CaSiO}_4$  [50]. Obviously, the total mass loss of specimens increased with the increasing IBA content since the quantities of hydrated products was increased with the increasing IBA content. In addition, the peaks around 150 °C in DTG curves of UHPC incorporating IBA were higher and wider compared to the reference sample, which indicated the larger amount of hydrates than that of the reference sample. The mass loss around 450 °C of UHPC incorporating with IBA was lower than that of reference sample, and when 100% IBA was used, the amount of  $\text{Ca}(\text{OH})_2$  was 0.51%, which was 38% reduction compared to the reference sample. This was due to the increased hydration of OPC and pozzolanic reaction of SCMs and IBA, while the latter consumed more  $\text{Ca}(\text{OH})_2$  [54].

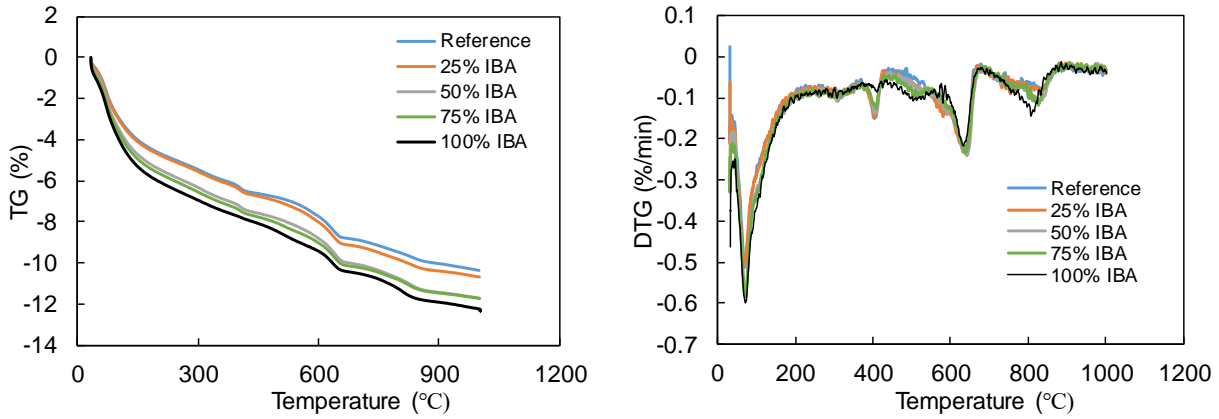


Figure 10 TG and DTG curves of UHPC incorporating different amounts of IBA

### 3.6 Pore structure

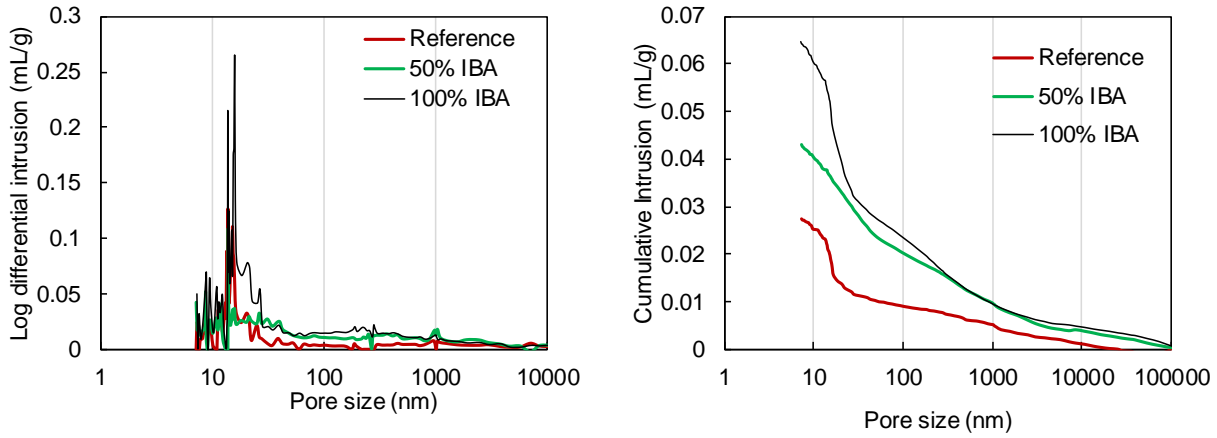
The pore structures of UHPC incorporating with 0%, 50% and 100% IBA are shown in Figure 11. The cumulative pore volume increased with the increasing amount of IBA due to the porous structure of IBA. The cumulative pore volume was increased from 0.028 mL/g to 0.068 mL/g when the content of IBA was increased from 0% to 100%. Usually, the compressive strength is closely related to the porosity of concrete and degree of hydration [55], and a lower porosity leads to a higher compressive strength. However, the present study showed that, the compressive strength increased firstly when the amount of IBA was less than 25%, then decreased obviously. Figure 11 also shows the pore size distribution of UHPC. The incorporation of IBA in the UHPC shifted the average pore size towards the larger sizes due to the presence of IBA. This was consistent with the microstructural observations. The coarsening effect was more pronounced as the content of IBA increased.

The BET results are shown in Figure 12. It can be observed that the total porosity of UHPC increased significantly with increasing amounts of IBA. The main peaks at about 10 nm shifted to the right as the amount of IBA increased. Similar to the MIP results, the addition of IBA shifted the average pore diameter towards to the larger size. From results in Figure 13(a), it is obvious that

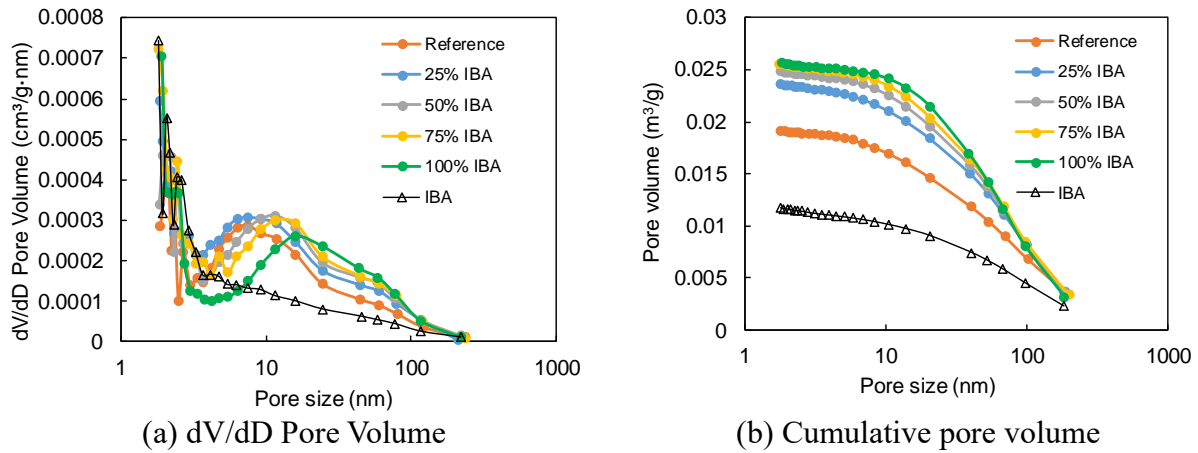
not only the total pore volume was increased, but also the volume of pore less than 50 nm increased. The pores less than 50 nm refer to gel-meso pores [56]. Meanwhile, the pore structure of pure IBA was also separately tested by nitrogen adsorption method, and the pore volume was only 0.01175 m<sup>3</sup>/g (shown in Figure 12). Compared to the water adsorption value of IBA, the pore volume tested by the BET method was much less than the actual pore volume. So much pores in IBA were larger than 200 nm, which could not determine by nitrogen adsorption method. Therefore, the addition of IBA showed lower improvement of porosity obtained from nitrogen adsorption method than that of MIP results.

In order to clearly understand the beneficial effect of IBA on the refinement of pores in UHPC matrix, the pore size distribution of UHPC matrix with and without IBA was further analyzed. The pore size distribution was divided into three ranges of size based on a previous study: The gel-meso pores with sizes less than <50 nm, the medium capillary pores with size range from 50-100 nm and the large capillary pores with a size larger than 100 nm [56]. As the pore structure and content of IBA were known, the pore structure of UHPC paste (matrix) can be obtained by excluding the pores from IBA. The amount of different sizes of pores in each UHPC matrix are shown in Figure 13 (b). It can be seen that the pore size distribution and porosity of UHPC matrix was changed after replacing the quartz sand with IBA. The porosity of UHPC matrix was obviously reduced by adding IBA. The pore volumes of gel-meso pores (<50 nm) and medium capillary pores (50-100 nm) in the UHPC matrix were also significantly reduced. However, the large capillary pores of UHPC were significantly increased due to the porous IBA (shown in Figure 12). The porous IBA contributed to the initial large pores of UHPC, while the internal curing of IBA promoted the hydration of the paste and reduced the large and medium pores in the paste. On one hand, the amount of hydration products was increased by incorporating IBA, which filled the large

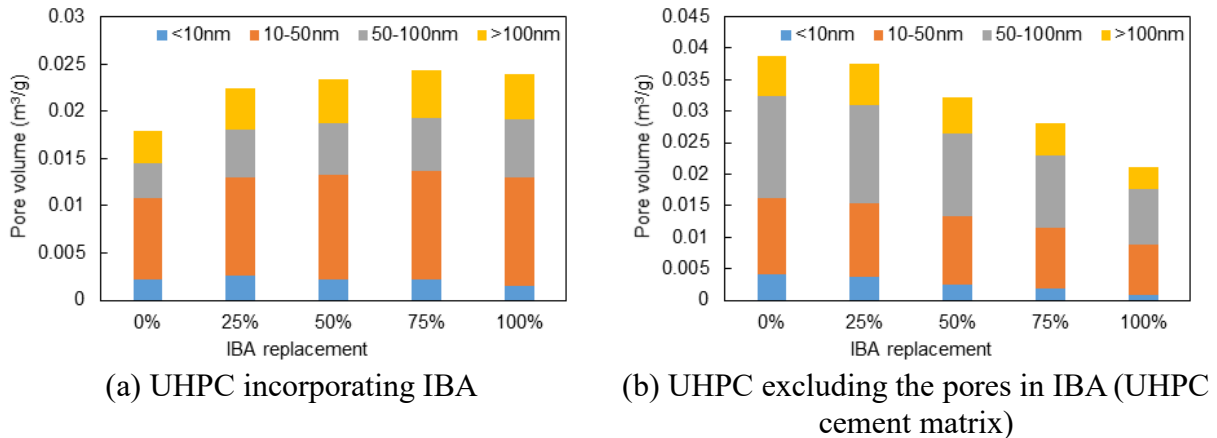
341 and medium pores. But on the other side, the IBA itself contained a lot of large pores, which  
 342 coarsened the pore size distribution of UHPC.



(a) Log differential intrusion (b) Cumulative pore volume  
 Figure 11 MIP pore structures of UHPC incorporating different amounts of IBA



(a) dV/dD Pore Volume (b) Cumulative pore volume  
 Figure 12 Pore structure of UHPC and IBA tested by nitrogen adsorption method



(a) UHPC incorporating IBA (b) UHPC excluding the pores in IBA (UHPC cement matrix)  
 Figure 13 Pore volume distributions: gel pores, medium capillary pore and large capillary pores (from nitrogen adsorption results)

## 4. Further discussion

### 4.1 Compressive strength enhancement of UHPC incorporating a small amount of IBA

In this study, the compressive strength of UHPC incorporating with 25% IBA was the highest compared to other specimens. This is contrary to the general understanding that because the IBA was a porous material with a low hardness and poor mechanical properties, the incorporated IBA in the UHPC would lead to a lower compressive strength. There were several factors that contributed to the enhancement of compressive strength. From the hydration heat results, the presoaked water in IBA promoted the hydration of UHPC, leading to a higher hydration degree. More hydration products were produced, which made the matrix of UHPC denser and more impermeable compared to the reference sample (see in Figure 11 and Figure 13 (b)). In addition, the micro-mechanical properties of matrix in UHPC incorporated IBA was improved (shown in Figure 9). The matrix acted as a dense barrier surrounding IBA. Also, the pozzolanic reaction (although slow) between the IBA and  $\text{Ca}(\text{OH})_2$  produced from the hydration of OPC also produced a limited amount of additional C-S-H [57, 58]. Although the total porosity of UHPC was increased after adding IBA, the enhancement of the microstructure due to the internal curing and pozzolanic effect overwhelmed the adverse effect of the porous IBA when the amount of IBA was small. As a result, the compressive strength was enhanced. For UHPC incorporating 50%, 75% and 100% IBA, the reduction of compressive strength due to increased porosity is higher than the enhancement of compressive strength due to internal curing. Thus, the compressive strength of UHPC incorporating less than 25% IBA could achieve a highest value.

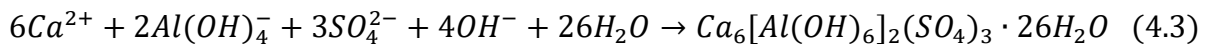
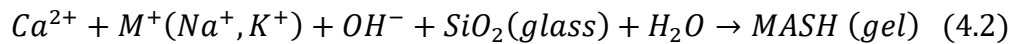
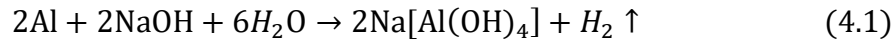
### 4.2 Expansion behavior vs. UHPC characteristics

Based on the above results, the reasons why the incorporated IBA had limited influence on volume stability of UHPC are as follows:



(1) High autogenous shrinkage of UHPC and relatively low humidity

Normally, the low water to binder ratio used in UHPC results in a lower internal relative humidity (less than 100%) [25]. The pores in UHPC are unsaturated, and the presence of pore solution menisci can lead to self-desiccation [59]. As a result, autogenous shrinkage is relatively high, and according to a previous study, an autogenous shrinkage value of about 2000  $\mu\epsilon$  can be developed at 7 d [26]. In the present study, the autogenous shrinkage of the paste mitigated by the expansion induced by the reactions of the metallic Al, glass and gypsum in the IBA. The chemical reactions of metallic Al, glass and gypsum in concrete can be expressed by Equations (4.1), (4.2) and (4.3). It can be noted that the reaction of metallic Al and gypsum would consume a large amount of water. However, the relative humidity of UHPC decreased rapidly at the early age [26], thus free water was not available for these reactions. Apparently, these reactions would be limited by the relatively low humidity. Overall, the expansive reaction of IBA in UHPC slowed down, and the limited expansion might be compensated by the rapid development of autogenous shrinkage.



(2) High content of SCMs

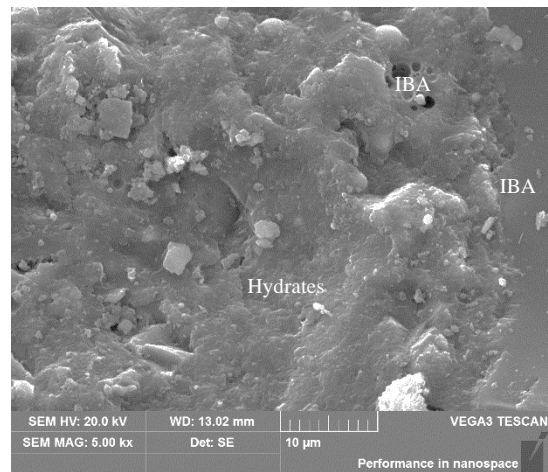
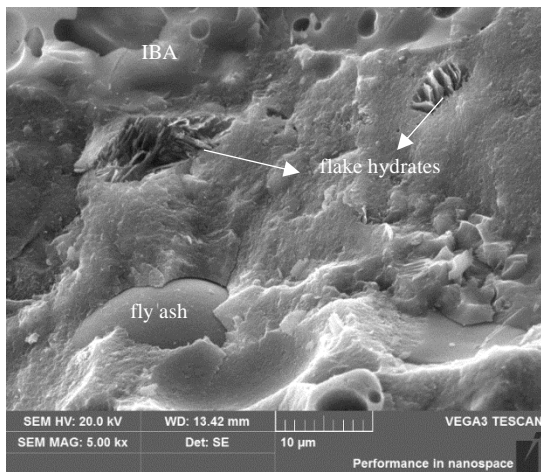
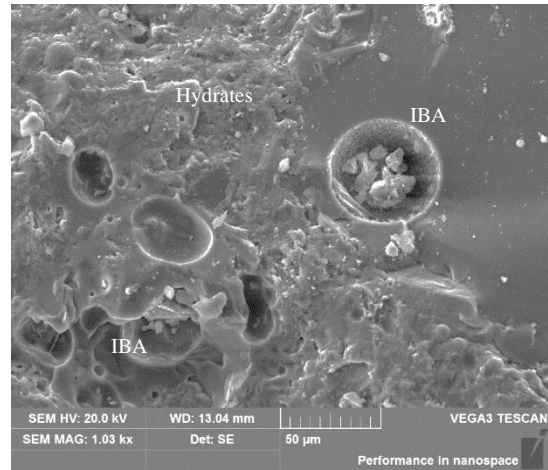
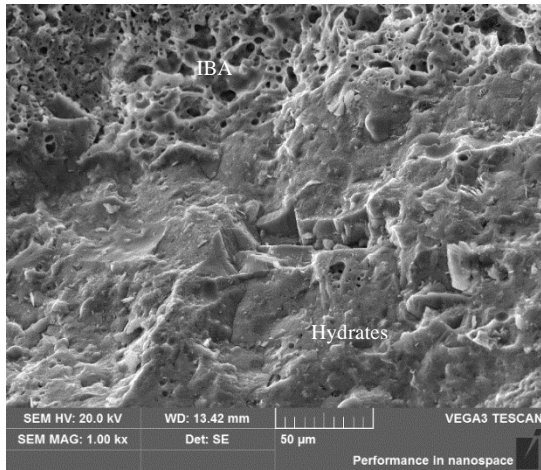
In this study, the UHPC contained a large amount of silica fume and fly ash, which was proven in previous studies to mitigate the ASR expansion of aggregates effectively [60]. Since there were some glass residues in IBA, the reduced ASR expansion was mainly attributed to the reduced alkalinity due to the dilution effect, pozzolanic reaction of SCMs and refinement of microstructure by filling effect [61]. It should be noted that the reduction of alkalinity of the pore solution could further hinder the possible reaction of metallic aluminum and gypsum. In addition,

the pozzolanic reaction was enhanced due to the internal curing effect of IBA, which can further reduce the possibility of expansion reaction.

### (3) Dense microstructure of UHPC

Compared to the pore structure of conventional concrete, the UHPC has much lower porosity and a higher fraction of fine pores ranging between 5 nm and 50 nm [26]. The reduction in porosity of the paste can probably lead to the low transport properties of UHPC, which renders the infiltration of foreign materials into the microstructure difficult. It should be noted that the microstructure of cement paste of UHPC was densified by the internal curing of IBA (shown in Figure 13), which could further hinder the transport of foreign ions. Hence, the reactions of metallic Al, glass and gypsum in 1 M NaOH solution were slowed down. In addition, most of the pores in the UHPC matrix were gel-meso pores with the size of less than 50 nm (shown in Figure 13). The smaller amount of capillary pores also hindered these chemical reactions because the expansive products did not have space to grow. Meanwhile, the capillary pores were not saturated due to relative low humidity [26], which further hindered these chemical reactions.

Generally, there was a high risk of crack due to expansion when the IBA was used as aggregates in conventional concrete [21, 62, 63]. In this study, the expansion caused by IBA in UHPC was restricted effectively. After immersing in 1 M NaOH solution for 28 d, there was no macro-crack or spalling damage observed in UHPC incorporating with 100% IBA (shown in Figure 14). But there were some flake and loose hydrates could be observed. Overall, the expansive reactions due to the presence of metallic Al, glass and gypsum were innocuous due to the impermeable paste, the presence of SCMs, high self-desiccation and high early strength. Therefore, the expansion risks of IBA in concrete can be disregarded when it was used in UHPC system.



UHPC incorporating with 100% IBA after immersing in NaOH for 28d

UHPC incorporating with 100% IBA before immersing in NaOH

Figure 14 Morphologies of UHPC incorporating IBA before and after immersing in NaOH solution

## 5. Conclusion

In this study, the effects of IBA on the mechanical properties, workability, hydration, microstructure and volume stability of UHPC were systemically investigated. The mechanisms governing the mechanical properties and volume stability of UHPC incorporating with IBA were explored. Based on the results and discussions in this study, the following conclusion can be drawn.

(1) The presoaked IBA had little influence on the workability of UHPC. The hardened density of UHPC decreased with the increasing replacement of IBA. The addition of a small amount of IBA (less than 25%) could improve the compressive strength of UHPC due to the internal curing effect of IBA, while using a large amount of IBA reduced the strength significantly.

(2) The internal curing of IBA promoted the hydration of UHPC paste, leading to a higher hydration degree. The pozzolanic reaction of silica fume and fly ash was improved, consuming more  $\text{Ca}(\text{OH})_2$  in UHPC. Thus, in the case of UHPC incorporating with IBA, the pore structure of the cement matrix became finer and the micro-hardness was increased. Therefore, the refinement of pore structure and reduced porosity of UHPC matrix could counterbalance the adverse effect caused by the porous structure of IBA. This contributed to the enhancement of compressive strength of UHPC incorporating an appropriate amount of IBA.

(3) The dry shrinkage was increased with the increased addition of IBA due to the increase of the total water to binder ratio of UHPC. The volume stability of UHPC after immersion in hot NaOH solution was shifted from shrinkage to expansion as the content of IBA increased, but the maximum expansion was only 196.5  $\mu\text{ε}$  when 100% IBA was used. Thus the study demonstrated that expansive reactions due to the presence of metallic Al, glass and gypsum in IBA were innocuous due to the impermeable nature of the UHPC paste, the presence of SCMs, a high self-desiccation, high early strength and small particle size of IBA. Hence, the reuse of IBA in UHPC was feasible solution for recycling IBA.

Based on the test results, it is possible to reuse IBA in UHPC without considering the expansive risks of IBA. The appropriate percentage of IBA as replacement of sand in UHPC without adverse effect on its performance is less than 25%. In addition, the IBA may possess some pozzolanic reactivity [57], demonstrating the potential to be used as SCMs in UHPC. So, the research on the performance of UHPC incorporated with ground IBA powders is of interest to be studied in future research. Meanwhile, more detailed studies should be performed to investigate the internal curing effect of IBA in UHPC.

## Acknowledgements

The authors wish to acknowledge the financial supports from the Innovation Technology Fund and the Environment and Conservation Fund of Hong Kong.

## References

- [1] A. Keulen, Z.A. Van, P. Harpe, W. Aarnink, H.A. Simons, H.J. Brouwers, High performance of treated and washed MSWI bottom ash granulates as natural aggregate replacement within earth-moist concrete, *Waste Management* 49 (2016) 83-95.
- [2] N. Holmes, H. O'Malley, P. Cribbin, H. Mullen, G. Keane, Performance of masonry blocks containing different proportions of incinerator bottom ash, *Sustainable Materials & Technologies* 8 (2016) 14-19.
- [3] M. Xu, B. Lin, Exploring the “not in my backyard” effect in the construction of waste incineration power plants-based on a survey in metropolises of China, *Environmental Impact Assessment Review* 82 (2020) 106377.
- [4] Environmental Protection Department (EPD), <https://www.epd.gov.hk/epd/english/top.html>, 2018.
- [5] P. Tang, M. Florea, P. Spiesz, H. Brouwers, Characteristics and application potential of municipal solid waste incineration (MSWI) bottom ashes from two waste-to-energy plants, *Construction and Building Materials* 83 (2015) 77-94.
- [6] C.R. Cheeseman, S.M.D. Rocha, C. Sollars, S. Bethanis, A.R. Boccaccini, Ceramic processing of incinerator bottom ash, *Waste Management* 23(10) (2003) 907-916.
- [7] R. Siddique, Use of municipal solid waste ash in concrete, *Resources Conservation & Recycling* 55(2) (2011) 83-91.
- [8] Lidelöw, Sofia, Anders Lagerkvist, Evaluation of leachate emissions from crushed rock and municipal solid waste incineration bottom ash used in road construction, *Waste Management* 27(10) (2007) 1356-1365.
- [9] T. Astrup, A. Muntoni, A. Poletini, R. Pomi, T. Van Gerven, A. Van Zomeren, Treatment and Reuse of Incineration Bottom Ash, (2016) 607-645.
- [10] Z. Av, R.N. Comans, Carbon speciation in municipal solid waste incinerator (MSWI) bottom ash in relation to facilitated metal leaching, *Waste Management* 29(7) (2009) 2059-2064.
- [11] P. Tang, M.V.A. Florea, P. Spiesz, H.J.H. Brouwers, Application of thermally activated municipal solid waste incineration (MSWI) bottom ash fines as binder substitute, *Cement & Concrete Composites* 70 (2016) 194-205.
- [12] X. Gao, B. Yuan, Q.L. Yu, H.J.H. Brouwers, Characterization and application of municipal solid waste incineration (MSWI) bottom ash and waste granite powder in alkali activated slag, *Journal of Cleaner Production* 164 (2017) 410-419.
- [13] D. Xuan, P. Tang, C.S. Poon, Effect of casting methods and SCMs on properties of mortars prepared with fine MSW incineration bottom ash, *Construction & Building Materials* 167 (2018) 890-898.
- [14] P. Tang, D. Xuan, C.S. Poon, D.C.W. Tsang, Valorization of concrete slurry waste (CSW) and fine incineration bottom ash (IBA) into cold bonded lightweight aggregates (CBLAs): Feasibility and influence of binder types, *J Hazard Mater* 368 (2019) 689-697.
- [15] K. Rubner, F. Haamkens, O. Linde, Use of municipal solid waste incinerator bottom ash as aggregate in concrete, *Quarterly Journal of Engineering Geology & Hydrogeology* 41(4) (2008) 459-464.
- [16] L. Su, G. Guo, X. Shi, M. Zuo, D. Niu, A. Zhao, Y. Zhao, Copper leaching of MSWI bottom ash co-disposed with refuse: effect of short-term accelerated weathering, *Waste management* 33(6) (2013) 1411-1417.

493 [17] J. Todorovic, H. Ecke, Treatment of MSWI Residues for Utilization as Secondary Construction  
 494 Minerals: A Review of Methods, Minerals & Energy - Raw Materials Report 20(3-4) (2006) 45-  
 495 59.

496 [18] H. Ecke, H. Sakanakura, T. Matsuto, N. Tanaka, A. Lagerkvist, State-of-the-art treatment  
 497 processes for municipal solid waste incineration residues in Japan, Waste Management & Research  
 498 18(1) (2010) 41-51.

499 [19] A. Poletti, R. Pomi, The leaching behavior of incinerator bottom ash as affected by accelerated  
 500 ageing, Journal of Hazardous Materials 113(1) (2004) 209-215.

501 [20] Z. Jing, N. Matsuoka, F. Jin, T. Hashida, N. Yamasaki, Municipal incineration bottom ash  
 502 treatment using hydrothermal solidification, Waste Management 27(2) (2007) 287-293.

503 [21] J.E. Aubert, B. Husson, A. Vaquier, Metallic aluminum in MSWI fly ash: quantification and  
 504 influence on the properties of cement-based products, Waste Management 24(6) (2004) 589-596.

505 [22] J. Pera, L. Coutaz, J. Ambroise, M. Chababbet, Use of incinerator bottom ash in concrete, Cement  
 506 & Concrete Research 27(1) (1997) 1-5.

507 [23] N. Saikia, G. Mertens, K.V. Balen, J. Elsen, T.V. Gerven, C. Vandecasteele, Pre-treatment of  
 508 municipal solid waste incineration (MSWI) bottom ash for utilisation in cement mortar,  
 509 Construction & Building Materials 96(15 October) (2015) 76-85.

510 [24] D. Xuan, P. Tang, C.S. Poon, Limitations and quality upgrading techniques for utilization of  
 511 MSW incineration bottom ash in engineering applications – A review, Construction and Building  
 512 Materials 190 (2018) 1091-1102.

513 [25] P. Shen, L. Lu, Y. He, F. Wang, J. Lu, H. Zheng, S. Hu, Investigation on expansion effect of the  
 514 expansive agents in ultra-high performance concrete, Cement and Concrete Composites (2019)  
 515 103425.

516 [26] P. Shen, L. Lu, F. Wang, Y. He, S. Hu, J. Lu, H. Zheng, Water desorption characteristics of  
 517 saturated lightweight fine aggregate in ultra-high performance concrete, Cement and Concrete  
 518 Composites 106 (2020) 103456.

519 [27] E. Ferraz, S. Andrejkovičová, W. Hajjaji, A.L. Velosa, A.S. Silva, F. Rocha, Pozzolanic activity  
 520 of metakaolins by the French Standard of the modified Chapelle Test: A direct methodology, Acta  
 521 Geodyn. Geomater 12(3) (2015) 289-298.

522 [28] R. Yu, P. Spiesz, H.J.H. Brouwers, Mix design and properties assessment of Ultra-High  
 523 Performance Fibre Reinforced Concrete (UHPFRC), Cement and Concrete Research 56 (2014)  
 524 29-39.

525 [29] G. Hüsken, A multifunctional design approach for sustainable concrete: with application to  
 526 concrete mass products, Eindhoven, The Netherlands: Eindhoven University of Technology  
 527 (2010).

528 [30] C. ASTM, Standard test method for density and void content of hardened pervious concrete,  
 529 Annual book of ASTM standards, American Society for Testing and Materials (2012).

530 [31] B. EN, Methods of test for mortar for masonry–Part 3: Determination of consistence of fresh  
 531 mortar (by flow table), (1999).

532 [32] B. ISO, 8. Determination of drying shrinkage of concrete for samples prepared in the field or in  
 533 the laboratory, British Standard Institution (2009).

534 [33] Standard Test Method for Potential Alkali Reactivity of Aggregates (Mortar-Bar Method),  
 535 ASTM International, 2014.

536 [34] R. Yu, P. Tang, P. Spiesz, H.J.H. Brouwers, A study of multiple effects of nano-silica and hybrid  
 537 fibres on the properties of Ultra-High Performance Fibre Reinforced Concrete (UHPFRC)  
 538 incorporating waste bottom ash (WBA), Construction and Building Materials 60 (2014) 98-110.

539 [35] M. Valipour, K.H. Khayat, Coupled effect of shrinkage-mitigating admixtures and saturated  
540 lightweight sand on shrinkage of UHPC for overlay applications, *Construction and Building*  
541 *Materials* 184 (2018) 320-329.

542 [36] W. Meng, K. Khayat, Effects of saturated lightweight sand content on key characteristics of  
543 ultra-high-performance concrete, *Cement & Concrete Research* 101 (2017) 46-54.

544 [37] J. Justs, M. Wyrzykowski, D. Bajare, P. Lura, Internal curing by superabsorbent polymers in  
545 ultra-high performance concrete, *Cement and Concrete Research* 76 (2015) 82-90.

546 [38] S. Nie, S. Hu, F. Wang, P. Yuan, Y. Zhu, J. Ye, Y. Liu, Internal curing – A suitable method for  
547 improving the performance of heat-cured concrete, *Construction & Building Materials* 122 (2016)  
548 294-301.

549 [39] S. Nie, S. Hu, F. Wang, C. Hu, X. Li, Y. Zhu, S. Nie, S. Hu, F. Wang, C. Hu, Pozzolanic reaction  
550 of lightweight fine aggregate and its influence on the hydration of cement, *Construction &*  
551 *Building Materials* 153 (2017) 165-173.

552 [40] A.M. Neville, *Properties of concrete*, 4th and final ed., Wiley, New York, 1996.

553 [41] D. Xuan, C.S. Poon, Removal of metallic Al and Al/Zn alloys in MSWI bottom ash by alkaline  
554 treatment, *J Hazard Mater* 344 (2018) 73-80.

555 [42] S. Yang, H. Cui, C.S. Poon, Assessment of in-situ alkali-silica reaction (ASR) development of  
556 glass aggregate concrete prepared with dry-mix and conventional wet-mix methods by X-ray  
557 computed micro-tomography, *Cement and Concrete Composites* 90 (2018) 266-276.

558 [43] B. Hasanzadeh, F. Liu, Z. Sun, Monitoring hydration of UHPC and conventional paste by  
559 quantitative analysis on Raman patterns, *Construction and Building Materials* 114 (2016) 208-214.

560 [44] D. Wang, C. Shi, Z. Wu, J. Xiao, Z. Huang, Z. Fang, A review on ultra high performance concrete:  
561 Part II. Hydration, microstructure and properties, *Construction and Building Materials* 96 (2015)  
562 368-377.

563 [45] G. Espinoza-Hijazin, M. Lopez, Extending internal curing to concrete mixtures with W/C higher  
564 than 0.42, *Construction & Building Materials* 25(3) (2011) 1236-1242.

565 [46] P.M. Halleck, D.P. Bentz, Water Movement during Internal Curing: Direct observation using X-  
566 ray microtomography, *Concrete International Design & Construction* 28(10) (2006) 39-50.

567 [47] P. Shen, L. Lu, Y. He, M. Rao, Z. Fu, F. Wang, S. Hu, Experimental investigation on the  
568 autogenous shrinkage of steam cured ultra-high performance concrete, *Construction & Building*  
569 *Materials* 162 (2018) 512-522.

570 [48] P. Shen, W. Chen, L. Lu, H. Geng, Q. Li, Effect of aggregate exposing and curing agent on the  
571 performance of exposed aggregate concrete, *Construction & Building Materials* 156 (2017) 675-  
572 683.

573 [49] C. Shi, Z. Wu, J. Xiao, D. Wang, Z. Huang, Z. Fang, A review on ultra high performance concrete:  
574 Part I. Raw materials and mixture design, *Construction and Building Materials* 101, Part 1 (2015)  
575 741-751.

576 [50] F.M. Lea, *The chemistry of cement and concrete*, utterworth-Heinemann, (2019).

577 [51] D.L. Kong, J.G. Sanjayan, Effect of elevated temperatures on geopolymer paste, mortar and  
578 concrete, *Cement and concrete research* 40(2) (2010) 334-339.

579 [52] Y. Fang, J. Chang, Microstructure changes of waste hydrated cement paste induced by  
580 accelerated carbonation, *Construction and Building Materials* 76 (2015) 360-365.

581 [53] J. Chang, Y. Li, M. Cao, Y. Fang, Influence of magnesium hydroxide content and fineness on  
582 the carbonation of calcium hydroxide, *Construction and Building Materials* 55 (2014) 82-88.



- 583 [54] A. Poletini, S. Poletini, R. Pomi, P. Sirini, Physical properties and acid neutralisation capacity  
584 of incinerator bottom ash-portland cement mixtures, *Waste Management Series*, 1 (2000), 791-  
585 802.
- 586 [55] S. Collepardi, L. Coppola, R. Troli, M. Collepardi, Mechanical properties of modified reactive  
587 powder concrete, *ACI Special Publications* 173 (1997) 1-22.
- 588 [56] P.K. Mehta, P.J.M. Monteiro, I. ebrary, *Concrete: microstructure, properties, and materials*,  
589 McGraw-Hill New York (2006).
- 590 [57] X.C. Qiao, M. Tyrer, C.S. Poon, C.R. Cheeseman, Novel cementitious materials produced from  
591 incinerator bottom ash, *Resources, Conservation and Recycling* 52(3) (2008) 496-510.
- 592 [58] A. Poletini, R. Pomi, G. Carcani, The effect of Na and Ca salts on MSWI bottom ash activation  
593 for reuse as a pozzolanic admixture, *Resources, conservation and recycling* 43(4) (2005) 403-418.
- 594 [59] V.-T.-A. Van, C. Rößler, D.-D. Bui, H.-M. Ludwig, Rice husk ash as both pozzolanic admixture  
595 and internal curing agent in ultra-high performance concrete, *Cement and Concrete Composites*  
596 53 (2014) 270-278.
- 597 [60] H. Du, K.H. Tan, Use of waste glass as sand in mortar: Part II–Alkali–silica reaction and  
598 mitigation methods, *Cement and Concrete Composites* 35(1) (2013) 118-126.
- 599 [61] J.-X. Lu, B.-J. Zhan, Z.-H. Duan, C.S. Poon, Improving the performance of architectural mortar  
600 containing 100% recycled glass aggregates by using SCMs, *Construction and Building Materials*  
601 153 (2017) 975-985.
- 602 [62] U. Müller, K. Rübner, The microstructure of concrete made with municipal waste incinerator  
603 bottom ash as an aggregate component, *Cement and Concrete Research* 36(8) (2006) 1434-1443.
- 604 [63] L. Bertolini, M. Carsana, D. Cassago, A.Q. Curzio, M. Collepardi, MSWI ashes as mineral  
605 additions in concrete, *Cement and concrete research* 34(10) (2004) 1899-1906.

606